NANOSTRUCTURES AT LOW TEMPERATURES

Structure and magnetic properties of multi-walled carbon nanotubes modified with iron

G. E. Grechnev,[a)] V. A. Desnenko, A. V. Fedorchenko, A. S. Panfilov, and Yu. A. Kolesnichenko

B. Verkin Institute of Low Temperature Physics and Engineering, National Academy of Sciences of Ukraine, 47 Lenin Ave., Kharkov 61103, Ukraine

L. Yu. Matzui and M. I. Grybova

Kyiv National Taras Shevchenko University, Physical and Biological Faculties, 64 Volodymyrska Str., Kyiv 01601, Ukraine

Yu. I. Prylutskyy

Kyiv National Taras Shevchenko University, Physical and Biological Faculties, 64 Volodymyrska Str., Kyiv 01601, Ukraine and Technical University of Ilmenau, Institute of Physics, Laboratory of Chemistry, 09684 Ilmenau, Germany

U. Ritter and P. Scharff

Technical University of Ilmenau, Institute of Physics, Laboratory of Chemistry, 09684 Ilmenau, Germany
(Submitted July 14, 2010)
Fiz. Nizk. Temp. **36**, 1347–1351 (December 2010)

Magnetic properties of multi-walled carbon nanotubes modified with iron (MWCNT+Fe) are studied in detail in the temperature range 4.2–300 K. Carbon encapsulated Fe nanoparticles were produced by chemical vapor deposition. Low-temperature SQUID magnetization measurements are supplemented by structural studies employing thermogravimetric (TG) analysis, transmission electron microscopy (TEM), x-ray diffraction spectroscopy (XRD), and scanning electron microscopy (SEM). The magnetic susceptibility of MWCNT+Fe was also studied above room temperature to provide a complete picture of its magnetic phase transitions. [doi:10.1063/1.3530422]

INTRODUCTION

Carbon nanotubes (CNT) exhibit unique physical properties;[1,2] in particular, they are chemically and thermally stable, and are characterized by high mechanical strength, and thermal and electrical conductivity, as well as a large specific surface area. Now CNT are regarded as the most attractive building blocks for nanoelectronics: they are able to form a perfect spin-transport medium, since electron transport in them is one-dimensional and ballistic with a long spin relaxation time and weak spin-orbital effects. In addition, even pure CNT, which are nonmagnetic materials, are characterized by giant magneto-resistance.[3,4] On the other hand, it is quite obvious that modifying CNT (intercalation, chemical surface modification, filling the internal cavities with different elements) should lead to significant differences in their electronic structure and properties.[5–7] In particular, encapsulated Fe nanowires are expected to exhibit excellent magnetic properties, such as uniaxial magnetic anisotropy and a high magnetic coercitivity, greater than that of bulk iron. Owing to the very large magnetic shape anisotropies which result, encapsulation of magnetic phases in CNT could stabilize magnetic order against thermal fluctuations in extremely small systems. Also, ferromagnetic nanoclusters are expected to have much better magnetic properties than bulk metals due to their single domain nature.[8]

It is, therefore, desirable to produce CNT with magnetic material inside the nanotubes in a specific and controlled way. Beyond the geometrical advantage of a quasi-one-dimensional CNT design, the carbon shells can provide effective protection against oxidation. This is especially important, since applications of ferromagnetic nanoclusters are limited by oxidation in air. Finally, beyond the interest in practical applications, studies of these magnetic systems provide a way of exploring the physics of magnetic ordering in close-to-one-dimensional structures. In particular, it becomes possible to address a number of fundamental questions about the role of spin degrees of freedom in quantum wires or Luttinger liquids, where specific effects associated with spin-charge separation are expected.

This is a study of the structure of multi-walled CNT (MWCNT) modified with iron and their magnetic characteristics (magnetic susceptibility and magnetization) as functions of magnetic field and temperature. This makes it possible to detect and distinguish different iron phases and their spatial distribution in MWCNT with encapsulated Fe fabricated in our laboratory.

I. EXPERIMENTAL

Chemical vapor deposition (CVD) was used to produce CNT filled with iron. In thermal CVD a conventional heat

source is used, such as a resistive or inductive heater, a furnace or an IR lamp. Basically, the growth process involves heating a catalyst material to high temperatures in a tube furnace. This is followed by passing a hydrocarbon gas (the carbon source) through the tube reactor for a chosen growth time. Then, the system is cooled down to room temperature in a flow of inert gas to prevent oxidation of the carbon products. Finally, the carbonaceous materials grown over the catalyst are collected.

In the course of CNT growth the key parameters are the chosen hydrocarbons and catalysts, and the growth temperature. Together they determine the properties of the nanotubes. Our method is based on catalytic decomposition of benzene (as the carbon source) and ferrocene (source of iron) in a tube furnace at different temperatures. To fill the reactor volume simultaneously with the components, the experimental set-up includes an aerosol-generator and a tube furnace. A quartz glass tube (length 70 cm, diameter 3 cm) is preheated to a temperature between 800 and 950 °C. The aerosol generator is made of quartz glass and operates on a spray-aerosol principle. Argon is used as a carrier gas for feeding the reactor with an aerosol of benzene and ferrocene. The aerosol flow rate is varied between 4 and 5 L/min of argon. In the process the ferrocene decomposes and provides the iron particles required for nucleation of the CNT. After the reaction, iron clusters are found inside the CNT, whereas the aligned nanotubes grow on the quartz glass reactor wall. The reaction time mainly determines the length of the tubes. The CNT used in the experiments were produced with a reaction time of 10–20 min. At the end of the reaction the aerosol generator is shut down and the reactor is cooled in an argon flow (0.5 L/min; cooling time 5 h). Beyond the furnace temperature and the flow rate, the ferrocene concentration has the greatest effect on diameters of the CNT, as well as on the iron clusters contained in the nanotubes. The highest concentration of ferrocene we used was 5 wt %, but the concentration can be reduced to a level of 0.2 wt %. Such low concentrations of ferrocene lead to a decreased amount of iron inside the tubes, according to thermogravimetric (TG) analysis and transmission electron microscopy (TEM). A high concentration of ferrocene leads to crystallization of ferrocene on the spray nozzle and reduces the possible reaction time to a few minutes. A higher ferrocene concentration also leads to greater number of iron clusters in the reactor, and these iron nanoclusters have a larger diameter. The diameters of the formed CNT appear to be directly related to the diameters of the iron clusters. Therefore, one can obtain an increased CNT diameter by increasing the ferrocene concentration.

The structure and phase composition were studied by thermogravimetric analysis (TG, Satorius), x-ray diffraction spectroscopy (XRD) with an x-ray diffractometer (Bruker AXS), scanning electron microscopy (SEM, Philips FEI), and transmission electron microscopy (TEM, Philips TECNAI).

In the low-temperature range (4.2–290 K) the magnetic properties of the iron filled CNT were studied with a SQUID magnetometer for fields up to 50 kOe. For the magnetization studies, samples were prepared by compacting Fe-encapsulated CNT powder inside an elongated aluminum foil cylinder with diameter of 1.5 mm and about 7 mm in length. In all the measurements the applied magnetic field was aligned along the cylinder axis in order to minimize the effect of the demagnetization factor on the magnetization data. The magnetization measurements were made after cooling the sample from room to helium temperatures in zero magnetic field (zero-field-cooled, ZFC) and in the measured fields (field-cooled, FC). Then the temperature dependences of the magnetization $M(T)$ were measured with slow heating at a rate of about 1.5 K/min in applied magnetic fields $H = 0.3$, 5 and 30 kOe. The field dependence of the magnetization was also measured at $T = 4.2$ K in the ZFC regime for magnetic fields of up to 40 kOe.

The magnetic susceptibility of MWCNT+Fe was also measured above room temperature to provide a complete picture of its magnetic phase transitions. The Faraday technique was employed in magnetic fields of about 20 kOe upon heating and cooling of the specimens. The heating and cooling rates did not exceed 10 K/min.

II. RESULTS AND DISCUSSION

The TG results in Fig. 1 show that the overall iron content in the CNT sample is about 4.6 wt %. The TG data also demonstrate that quality of the CNT is very high, with a very low amount of amorphous carbon. Decomposition of the CNT starts at temperature about 570 °C.

According to the electron microscopy data in Figs. 2 and 3, the CNT are MWCNT. The inner diameter of the MWCNT is 5–8 nm, while the outer diameter is about 40–60 nm and the length is up to 100 μm. This MWCNT contain clusters of iron (or its compounds) with average diameters of 10–15 nm and lengths of 120–140 nm.

X-ray diffraction patterns of MWCNT grown with benzene (BZ) are shown in Fig. 4. The peak at 26.1° corresponds to the interplanar spacing between the CNT walls and is marked as CNT (002). The interlayer spacing of 3.411 Å for nanotubes grown with BZ slightly exceeds that observed for the perfect graphite (3.354 Å). The intensity of the CNT (002) reflection is stronger in the case of the more tangled nanotubes grown with benzene than with other carbon sources. The other distinctive characteristic of CNT is the peak at $2\theta = 42.7°$, which corresponds to the (100) reflection.[9] A peak at $2\theta = 35.4°$ corresponds to the iron oxide

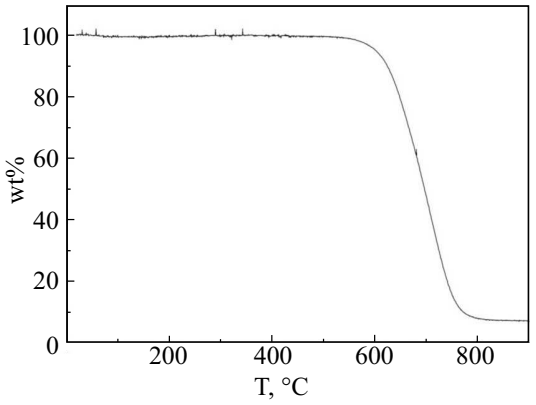

FIG. 1. Thermogravimetric measurements of MWCNT (starting mass 10.45 mg, rate 1°/min in air).

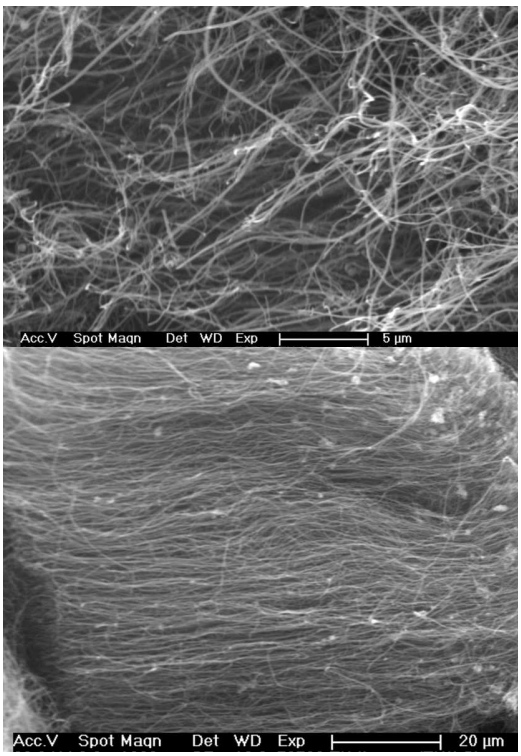

FIG. 2. SEM image of MWCNT modified with iron (ferrocene concentration 1 wt % in benzene).

(110) reflection.[10] The iron oxide (202) reflection at 42.6° is superimposed on a much stronger CNT (100) feature. Another peak in the recorded patterns is the iron carbide peak, IC (103), at $2\theta=44.8°$.[10,11] This iron carbide phase is presumably a residue of CNT growth due to precipitation of carbon feed from catalyst/hydrocarbon droplets.[11] Finally, the crystalline phase of α-Fe is represented by a strong (110) reflection, which is represented by an additional peak at 51.1°.[10]

The temperature dependences of χ obtained at a low field of 300 Oe in both the ZFC and FC regimes are presented in Fig. 5. The ZFC curve exhibits a conspicuous magnetic transition at temperatures slightly above 100 K. The shape and position of this feature resemble the so-called Ver-

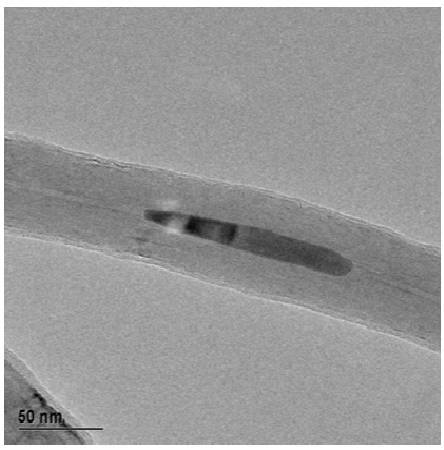

FIG. 3. TEM image of MWCNT modified with iron (ferrocene concentration 1 wt % in benzene).

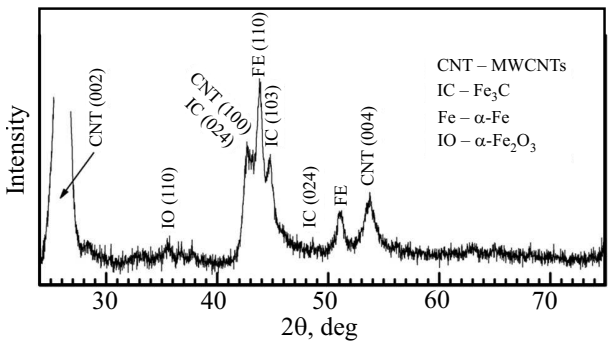

FIG. 4. XRD pattern for MWCNT modified with iron.

wey transition, which has been observed in the Fe_3O_4 oxide (magnetite) at $T_m=120$ K. This can be regarded as evidence of the presence of Fe_3O_4 nanoparticles in this sample. Moreover, the absence of a distinct decay of magnetization with temperature, as in superparamagnetic systems, also points to a large magnetic anisotropy energy, as well as to a substantial fraction of magnetic nanoparticles. The discrepancy between the ZFC and FC magnetization curves may imply a complex magnetic state at low temperatures, e.g., a spin-glass cluster state.

The temperature dependence of the magnetization at higher fields is shown in Fig. 6. One can see a nonmonotonic, step-like behavior in the temperature variation of the susceptibility $\chi(T)$ measured in a field of 5 kOe over 70–100 K. This behavior can be attributed to the appearance of a magnetic phase. This phase might exist in the iron nanoclusters, as in the recently indicated appearance of a γ-iron phase.[12] On the other hand, the observed feature may be related to a manifestation of exchange bias in larger particles. The measured temperature dependence of the magnetization in a field of 20 kOe is also shown in Fig. 6.

The field dependence of ZFC magnetization was measured at $T=4.2$ K and is shown in Fig. 7. The saturation magnetic moment at liquid helium temperature is 8.5 emu/g, as opposed to the value of 217 emu/g for the saturation magnetization of bulk iron. Assuming that encapsulated nanopar-

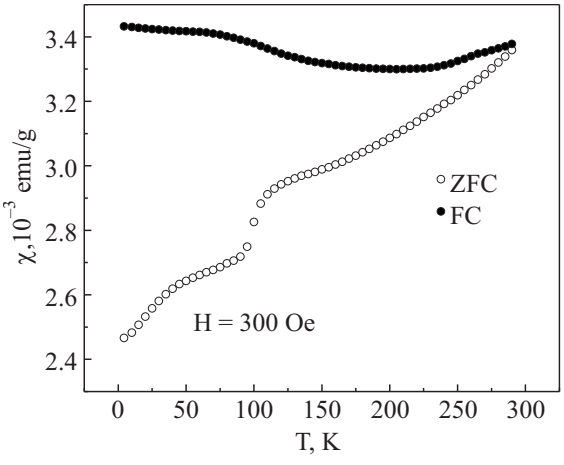

FIG. 5. Temperature dependence of the magnetic susceptibility for MWCNT modified with iron measured in the range 4.2–300 K in a field of 300 Oe in both the FC and ZFC regimes.

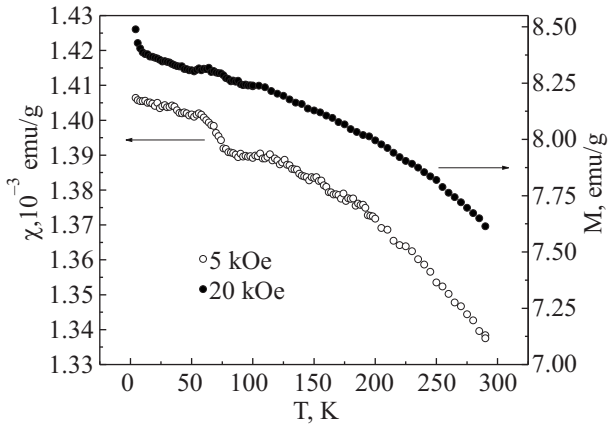

FIG. 6. Measured temperature dependences of the magnetic susceptibility and magnetization of MWCNT modified with iron for T=4.2–300 K in the ZFC regime at fields of 5 and 20 kOe, respectively.

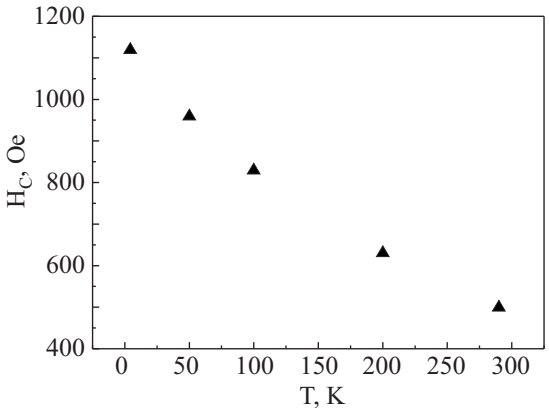

FIG. 8. Temperature dependence of the coercitivity for MWCNT modified with iron for T=4.2–300 K.

ticles consist predominantly of iron, one can estimate the fraction of the iron phase as 4%. The iron concentration in the sample was also estimated from the TG analysis as (4 ± 1) wt %. This result agrees with our magnetization analysis, which presumably yields the amount of magnetic material with greater precision. Since saturation occurs at fields just above 10 kOe, as shown in Fig. 7, this indicates a large magnetic anisotropy in the Fe-CNT system studied here.

The temperature dependences of the coercitivity H_C and residual magnetization M_R of our Fe-CNT sample were derived from the reversible curves of saturation magnetization and are shown in Figs. 8 and 9. The increases in H_C and M_R with decreasing temperature are evident. In particular, when the temperature is reduced from 300 to 4.2 K, the coercitivity increases by a factor of 2.3, and the residual magnetization also increased by a factor of 1.5. At liquid helium temperatures, H_C and M_R are equal to 1120 Oe and 2.95 emu/g, respectively.

The results of a supplementary study of the variation in the magnetic susceptibility $\chi(T)$ above room temperature are shown in Fig. 10. This figure clearly indicates a magnetic transition at about 480 K, which is presumably related to a cementite phase, with a Curie temperature of about 483 K for bulk Fe_3C.[13] At higher temperatures one can expect a superparamagnetic contribution from iron nanoclusters with a blocking temperature of about 500 K.

III. CONCLUSIONS

We have studied the structural and magnetic characteristics of Fe-MWCNT nanoclusters produced by catalytic decomposition of benzene and ferrocene. SEM and TEM studies show that the MWCNT have an inner diameter of about 5–8 nm, whereas the outer diameter is about 40–60 nm and the length is up to 100 μm; they contain clusters of iron (or its compounds) with average diameters of 10–15 nm and lengths of 120–140 nm. X-ray diffraction data reveal a number of iron and carbon phases in the Fe-MWCNT. The ZFC and FC temperature dependences of the magnetic susceptibility reveal a number of magnetic phase transitions in this Fe-MWCNT system, including a Verwey transition in Fe_3O_4 particles which are presumably outside the MWCNT. It has been shown that both the residual magnetization M_R and the coercive field H_C decrease monotonically with increasing temperature. The existence of a spin-glass state and interactions between nanoparticles of various sizes could contribute to the observed magnetic behavior.

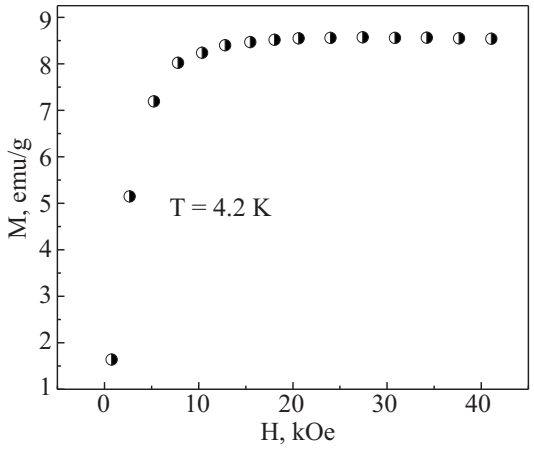

FIG. 7. Field dependence of the ZFC magnetization for MWCNT modified with iron measured at 4.2 K.

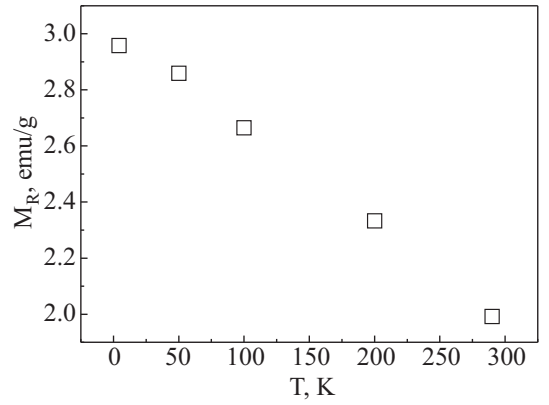

FIG. 9. Temperature dependence of the residual magnetization M_R for MWCNT modified with iron for T=4.2–300 K.

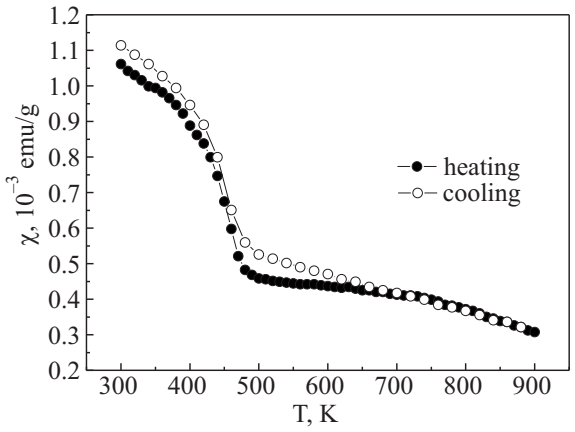

FIG. 10. Temperature dependences of the magnetic susceptibility for MWCNT modified with iron above room temperature.

a)Email: grechnev@ilt.kharkov.ua

[1]M. S. Dresselhaus, G. Dresselhaus, and P. C. Eklund, Science of Fullerenes and Carbon Nanotubes, New York: Academic Press (1996).
[2]P. J. F. Harris, Carbon Nanotubes and Related Structures, Cambridge: Univ. Press (1999).
[3]G. C. McIntosh, G. T. Kim, J. G. Park, V. Krstic, M. Burghard, S. H. Jhang, S. W. Lee, S. Roth, and Y. W. Park, Thin Solid Films **417**, 67 (2002).
[4]A. Cottet, T. Kontos, S. Sahoo, H. T. Man, M. S. Choi, W. Belzig, C. Bruder, A. F. Morpurgo, and C. Schonenberger, Semicond. Sci. Technol. **21**, 78 (2006).
[5]P. K. Tyagi, A. M. Manoj, K. S. D. Misraa, J. Ghatak, P. V. Satyam, and F. Le Normand, Appl. Phys. Lett. **86**, 253110 (2005).
[6]E. Borowiak-Palen, M. H. Ruemmeli, T. Gemming, T. Pichler, R. J. Kalenczuk, and S. R. P. Silva, Nanotechnology **17**, 2415 (2005).
[7]O. V. Mykhailenko, D. Hui, Y. M. Strzhemechny, D. Matsui, Yu. I. Prylutskyy, and P. Eklund, J. Comput. Theor. Nanosci. **4**, 1 (2007).
[8]N. Grobert, W. K. Hsu, Y. Q. Zhu, J. P. Hare, H. W. Kroto, D. R. M. Walton, M. Terrones, H. Terrones, P. Redlich, M. Ruehle, R. Escudero, and F. Morales, Appl. Phys. Lett. **75**, 3363 (1999).
[9]A. G. Kudashov, A. V. Okotrub, L. G. Bulusheva, I. P. Asanov, Y. V. Shubin, and N. F. Yudanov, J. Phys. Chem. B **108**, 9048 (2004).
[10]S. A. Ibitoye and A. A. Afonja, J. Miner. Mater. Char. & Eng. **7**, 203 (2008).
[11]U. Narkiewicz, N. Guskos, W. Arabczyk, J. Typek, T. Bodziony, and W. Konicki, Carbon **42**, 1127 (2004).
[12]A. Khasanov, J. He, J. Gaillard, K. Yang, A. M. Rao, C. M. Cameron, J. M. Schmeltzer, J. G. Stevens, and A. Nath, Appl. Phys. Lett. **93**, 013103 (2008).
[13]I. V. Ovsienko, L. Yu. Matzui, N. I. Zakharenko, N. G. Babich, T. A. Len, Yu. I. Prylutskyy, D. Hui, Yu. M. Strzhemechny, and P. C. Eklund, Nanoscale Res. Lett. **3**, 60 (2008).

This article was published in English in the original Russian journal. Reproduced here with stylistic changes by AIP.